

Photocatalysis

Tailoring the Optical Absorption of Water-Stable Zr^{IV}- and Hf^{IV}-Based Metal–Organic Framework PhotocatalystsTan L. H. Doan,^[a, b] Ha L. Nguyen,^[b] Hung Q. Pham,^[a, b] Nguyen-Nguyen Pham-Tran,^[a] Thach N. Le,^{*[a]} and Kyle E. Cordova^{*[b]}

Abstract: New Zr^{IV}- and Hf^{IV}-based metal–organic framework photocatalysts, termed VNU-1 and VNU-2 (where VNU = Vietnam National University), were synthesized and their resulting structures fully characterized. By employing a highly π -conjugated linker, namely 1,4-bis(2-[4-carboxyphenyl]ethyl)benzene, the optical absorption properties were effec-

tively red-shifted into the visible light region. This strategy, coupled with the high water stability of the materials, led to enhanced MOF-driven photocatalytic degradation, under ultraviolet-visible light, of organic dye pollutants commonly found in wastewater.

Introduction

The rapid advancement of the textile and dye industry, specifically in Vietnam, has led to serious concerns over the environmental effects of the wastewater generated. This wastewater most often contains toxic, environmentally unfriendly, and chemically stable organic dyes, which are difficult to degrade by standard biological treatments.^[1] Furthermore, organic dye waste poses significant challenges to the treatment of other pollutants as these molecules absorb and reflect sunlight, thus damaging the algal-bacterial growth needed for such treatment.^[2] An increasingly attractive method for degrading organic dye pollution in wastewater is the use of heterogeneous photocatalysts, which utilize sunlight to effectively eliminate the hazardous nature of organic pollutants and transform them into biodegradable or even less toxic molecules.^[3] Commonly used heterogeneous photocatalysts include metal oxides, such as TiO₂ and ZnO; however, these materials have drawbacks regarding their use for practical applications.^[4] First, the band gaps of these materials are rather large (~3.2 eV), which means that they primarily absorb light with wavelengths < 380 nm.^[4] These properties render them effective only in the UV region for photocatalytic or photodegradation applications. Second, these photocatalysts are generally suspended in aque-

ous solutions leading to inefficiency in recycling them for further use.^[5] Therefore, the development and exploration of new heterogeneous photocatalytic systems that can extend their function into the visible light region and can be effectively recycled are highly desired.

Metal–organic frameworks (MOFs) are a class of porous, crystalline materials constructed from inorganic clusters (termed secondary building units or SBUs) that are connected via organic linkers.^[6] These materials have attracted much interest for a wide range of applications, including gas storage and separation,^[6,7] carbon dioxide capture,^[8] heterogeneous catalysis,^[9] and chemical sensing,^[10] among others. MOFs have also received attention for their photocatalytic characteristics as they typically exhibit semiconductor properties upon exposure to light.^[11] It has been reported that the band gap of MOFs is closely associated to the HOMO–LUMO gap, which allows the light-harvesting properties of MOFs to be tailored through variation of the electronic nature of the inorganic SBUs and organic linkers comprising their structures.^[12,13] Although there have been a wide number of reported MOFs used for photocatalytic applications,^[11] there remains significant impediments to using these materials as photocatalysts in wastewater treatment due to the instability of these structures in aqueous environments.

In 2009, a water-stable and photoactive Ti-based MOF, termed MIL-125(Ti), was reported, in which the material's ability to photoinduce the oxidation of alcohols was demonstrated.^[14] Furthermore, with the report of a series of highly chemical- and water-stable MOFs based on Zr^{IV} clusters, termed UiO MOFs, attention has turned to exploring these materials in environments that were previously unsuitable for other MOF photocatalysts.^[15] Although these MOFs are stable in water, their photocatalytic properties are mainly applicable to the UV region as the linkers absorb light primarily at wavelengths < 300 nm.^[16] Integration of auxochromic and bathochromic

[a] T. L. H. Doan, H. Q. Pham, N.-N. Pham-Tran, Prof. T. N. Le
Faculty of Chemistry
University of Science, Vietnam National University
Ho Chi Minh City, 721337 (Vietnam)
E-mail: lenthach@yahoo.com

[b] T. L. H. Doan, H. L. Nguyen, H. Q. Pham, K. E. Cordova
Center for Molecular and NanoArchitecture (MANAR)
Vietnam National University
Ho Chi Minh City, 721337 (Vietnam)
E-mail: kcordova@manar.edu.vn

Supporting information for this article is available on the WWW under <http://dx.doi.org/10.1002/asia.201500641>.

functionalities, such as $-\text{NH}_2$ or $-\text{NO}_2$ groups, into the linkers of MIL-125(Ti)^[14,17] and UiO-66 and -67^[13c,16] has proven successful for shifting optical absorption from the UV to the visible-light region and, thus, enhancing practical photocatalytic properties. Alternative methods for increasing optical absorption in water-stable MOFs, proposed mainly through computational work, include increasing the π -conjugation of the linker backbone through introduction of additional aromatic rings or alkyne units.^[12,18,19] Indeed, this was recently realized by an isotreticular (having the same topology) UiO-66 structure constructed from a chromophoric anthracene-derived linker.^[20]

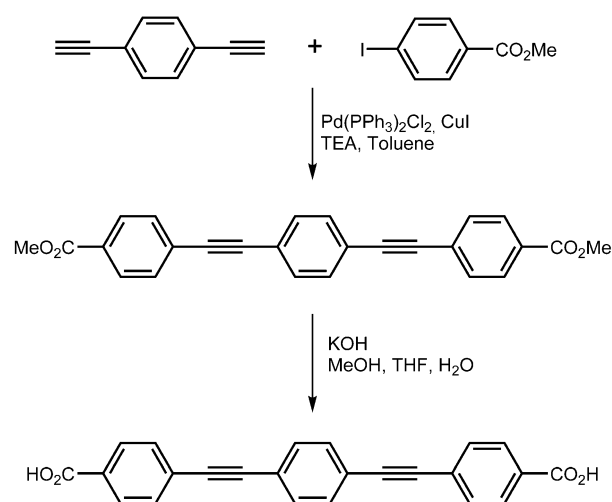
In this study, we demonstrate a strategy for further tailoring the optical absorption properties of a water-stable, Zr^{IV} -based MOF through increasing the π -conjugation of the linker. Specifically, we report the synthesis and structural characterization of a new Zr-MOF, termed VNU-1 (VNU = Vietnam National University), that was constructed from the ditopic linker 1,4-bis(2-[4-carboxyphenyl]ethynyl)benzene (H_2CPEB). Furthermore, the successful preparation of an isotreticular structure based on Hf-clusters, termed VNU-2, is presented. Due to the increase in conjugation of the linker, the absorption edge of VNU-1 was effectively red-shifted into the visible-light region. This finding led to the discovery of enhanced photocatalytic degradation under UV/Vis light of the environmentally malignant methylene blue (MB) and methyl orange (MO) dyes. It is noted that the photocatalytic activity of VNU-1 was significantly higher in comparison to the widely used Degussa P-25 TiO_2 photocatalyst.

Results and Discussion

Synthesis and structural characterization

To obtain a MOF with optical absorption properties extending to the visible-light region, we prepared a highly π -conjugated linker, termed H_2CPEB , based on a Sonogashira-coupling strategy that was adopted accordingly from a previous report (Scheme 1).^[21] With this in hand, VNU-1 and VNU-2 were solvothermally synthesized through a reaction containing H_2CPEB and $\text{ZrOCl}_2 \cdot 8\text{H}_2\text{O}$ or HfCl_4 , respectively, in *N,N*-dimethylformamide (DMF) at 120°C with acetic acid added as a modulator. The crystallinity of VNU-1 and -2 was regulated by varying the amount of acetic acid modulator added as well as the length of the reaction time.^[22] Depending on the degree of modulator added, single crystals of VNU-1-SC and VNU-2-SC (where SC = single crystal) as well as a microcrystalline powder (VNU-1-P and VNU-2-P, respectively; where P = powder) were obtained.

Single-crystal X-ray diffraction analysis revealed that VNU-1-SC and VNU-2-SC crystallized in the space group, *Fd-3m*, with $a = 39.8961$ and 39.7901 Å, respectively (Table 1, Tables S1 and S2 in the Supporting Information). These materials are isostructural to the PIZOF series, with the exception that the CPEB linker is not functionalized and VNU-2-SC is constructed from Hf^{IV} as opposed to Zr^{IV} .^[23] Specifically, both materials adopt a doubly interpenetrated **fcu-c** net based on $[\text{M}_6\text{O}_4(\text{OH})_4(\text{CO}_2)_{12}]$ ($\text{M} = \text{Zr}^{\text{IV}}$ or Hf^{IV} for VNU-1 or VNU-2, respectively) SBUs, in which the inner $\text{M}_6\text{O}_4(\text{OH})_4(\text{CO}_2)_{12}$ SBU cores are



Scheme 1. Synthesis of the highly π -conjugated ditopic linker, H_2CPEB , used to construct VNU-1 and VNU-2, was accomplished by a Sonogashira-coupling strategy (see section S1 in the Supporting Information).^[21]

| Table 1. Summary of crystallographic data for VNU-1-SC and VNU-2-SC. | | |
|--|--|--|
| | VNU-1-SC | VNU-2-SC |
| Empirical formula | $\text{C}_{72}\text{H}_{36}\text{Zr}_3\text{O}_{16}$ | $\text{C}_{72}\text{H}_{36}\text{Hf}_3\text{O}_{16}$ |
| Formula weight [g mol^{-1}] | 1430.67 | 1692.48 |
| T [K] | 298 | 100 |
| Crystal system | Cubic | Cubic |
| Space group | <i>Fd-3m</i> | <i>Fd-3m</i> |
| a [Å] | 39.8961(7) | 39.7901(8) |
| α [°] | 90 | 90 |
| Volume [Å ³] | 63 503(3) | 62 998(4) |
| Z | 16 | 16 |
| Calculated density, ρ_{calc} [g cm^{-3}] | 0.599 | 0.714 |
| Absorption coefficient, μ [mm^{-1}] | 1.821 | 3.793 |
| R_{int} | 0.0501 | 0.1295 |
| R_1 [$I > 2\sigma(I)$] | 0.0362 | 0.0283 |
| wR_2 | 0.1072 | 0.0726 |

ideally capped alternatively by $\mu_3\text{-O}$ and $\mu_3\text{-OH}$ groups to form the triangular faces (Figure 1). These SBUs are connected together by twelve carboxylate groups from CPEB linker units to produce both tetrahedral and octahedral cages (Figure 1 a, b). With respect to the two-fold interpenetration, the SBU of one **fcu** net occupies the center of the tetrahedral cages that belong to the second net (Figure 1 c). This results in one large tetrahedral cage (~ 25 Å) and one smaller octahedral cage (9 Å) (Figure 1 b). The total solvent-accessible volumes of VNU-1 and VNU-2, as determined by PLATON,^[24] are 68% for both of these structures.

As a result of the low yield obtained for reactions that produced single crystals, the amount of acetic acid modulator was reduced to obtain bulk microcrystalline powder phases for both VNU-1 and VNU-2 in higher yields. The purity of these bulk phases were assessed by powder X-ray diffraction (PXRD) measurements, in which the experimental as-synthesized PXRD patterns for both VNU-1-P and VNU-2-P were in satisfactory agreement to those patterns calculated for their respective single-crystal structures (Figure 2 a, Figure S5). Furthermore,

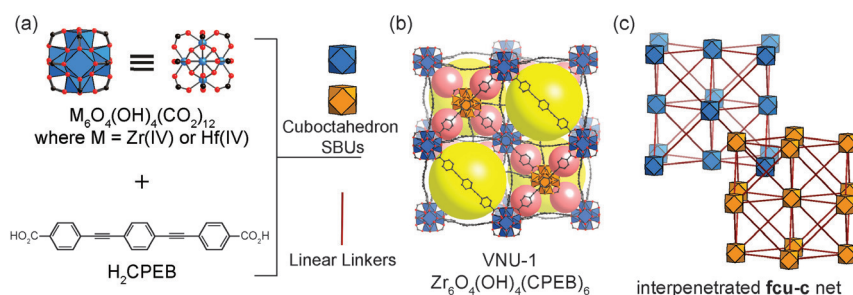


Figure 1. Crystal structure and topology of VNU-1 and -2: (a) Cuboctahedron $[M_6O_4(OH)_4(CO_2)_{12}]$ (where $M = Zr^{IV}$ or Hf^{IV} for VNU-1 or -2, respectively) secondary building unit (SBU) and H_2CPEB linear linker; (b) Crystal structure of VNU-1, as a representative example, showing the large 25 Å tetrahedral cages and smaller cages that result from the interpenetration of a second net; (c) Interpenetrated **fcu-c** net of VNU-1 and VNU-2 in which the cuboctahedron SBU of one net is located at the center of a tetrahedral cage belonging to the second net. It is noted that the SBU is replaced with cuboctahedron shapes, which are connected by linear-shaped linkers. Atom colors: Zr, blue and orange polyhedra; O, red; C, black; H atoms are omitted for clarity. The yellow and salmon colored balls represent the free space in the framework.

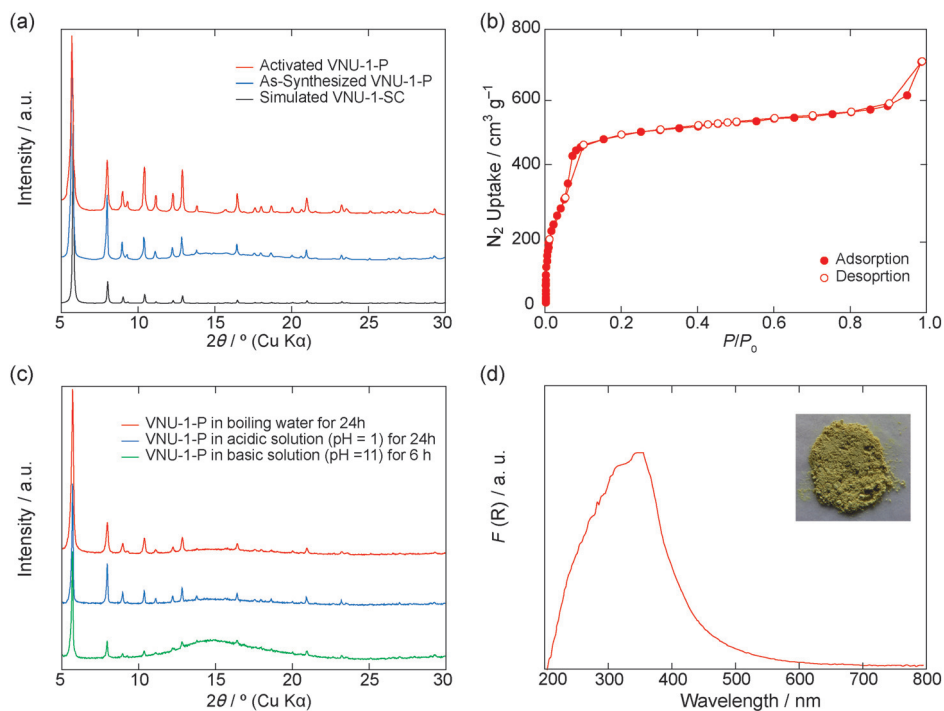


Figure 2. (a) PXRD analysis of VNU-1. The calculated pattern from the single-crystal data (black) is compared to the experimental patterns from the as-synthesized powder sample (blue) and activated powder sample (red). (b) N_2 isotherm at 77 K for activated VNU-1-P. Closed and open circles represent the adsorption and desorption branches, respectively. (c) PXRD analysis of VNU-1-P after immersing in a basic solution (pH 11) for 6 h (green), an acidic solution (pH 1) for 24 h (blue), and boiling water for 24 h (red). (d) UV-DRS spectrum of VNU-1-P. Inset: Optical image highlighting the yellow color of the material.

optical microscopy images taken for VNU-1-P and VNU-2-P displayed homogeneous crystal morphology, lending further support to the purity of the bulk phases (Figures S6 and S7). It is noted that microcrystalline powder samples, VNU-1-P and VNU-2-P, were used for all further characterizations and measurements as described below.

Architectural robustness and porosity

Prior to further characterization, as-synthesized samples of VNU-1-P and VNU-2-P were thoroughly washed with DMF to remove unreacted species and then solvent-exchanged with chloroform over the course of three days. Activation of chloroform-washed samples of VNU-1-P and VNU-2-P was performed under reduced pressure at 120 °C for 24 h. To assess the activation procedure as well as the architectural robustness of these two structures, thermal gravimetric analysis (TGA) was performed under air-flow. VNU-1-P and VNU-2-P exhibit a small decrease in weight percent up to the decomposition temperatures of 430 and 460 °C, respectively (Figures S8 and S9). After decomposition, the calculated weight percent of the residue was found to be 27.4 and 38.5% for VNU-1-P and VNU-2-P, respectively, which is in line with the theoretical values calculated from the crystal structures (25.3 and 36.9% for VNU-1-P and VNU-2-P, respectively). Furthermore, the calculated weight percent of the linker, as determined from the TGA curve, was found to be 72.6 and 63.2% for VNU-1-P and VNU-2-P, respectively. This weight percent is also consistent with those calculated from elemental microanalysis (73.5 and 63.8% for VNU-1-P and VNU-2-P, respectively). The porosity of both samples was established by N_2 isotherms at 77 K, which afforded type-IV behaviors due to the presence of mesopores within the structures (Figure 2b, Figure S10). The calculated Brunauer–Emmett–Teller

(Langmuir) surface areas of VNU-1-P and VNU-2-P were 2100 (2600) and 1700 (2100) $m^2 g^{-1}$, respectively. Following these findings, we sought to demonstrate the chemical and water stability of VNU-1-P, which functions as a representative example. As shown in Figure 2c, VNU-1-P remarkably maintains its crystallinity after being immersed in boiling water, in

an acidic solution (pH 1) for 24 h, as well as in a basic solution (pH 11) for 6 h.

Photoabsorption analysis

UV/Vis diffuse reflectance spectroscopy (UV-DRS) measurements were performed on activated samples of VNU-1-P and VNU-2-P (Figure 2d, Figure S11). As depicted in Figure 2d, the spectrum of VNU-1-P exhibits an intense absorption band at about 380 nm, whose edge extends to approximately 540 nm.^[25] This absorption in the visible-light region corresponds well with the yellow color of the powder sample (Figure 2d inset). The UV-DRS spectra of VNU-2-P and the original H₂CPEB linker display absorption band-edges of 369 nm and 320 nm, respectively (Figures S11 and S12). It is noted that the absorbance band-edge of VNU-1-P is significantly red-shifted in comparison to most other water-stable and photoactive MOFs, notably UiO-66,^[16,19] UiO-67,^[19] UiO-66-NO₂,^[13c] UiO-66-Br,^[13c] and MIL-125(Ti)^[13b,14] (Table 2). The optical band gaps of VNU-1-P and VNU-2-P were calculated to be 2.88 eV and 3.36 eV, respectively, based on the relationship $E_g = 1240/\lambda$ (Figure S13). At present, it is not clear as to why the CPEB linker did not positively influence the optical absorption properties of VNU-2-P, especially when considering that Hf and Zr have the same valence electron configurations.^[18]

To gain further understanding about the origins of the photoabsorption property in VNU-1-P, density functional theory calculations were employed to determine the electronic band structure and the density of states (DOS). These results are depicted in Figure 3. As is shown, the calculated theoretical band gap is 3.23 eV, which is slightly higher than the experimentally determined value. This discrepancy is acceptable since the

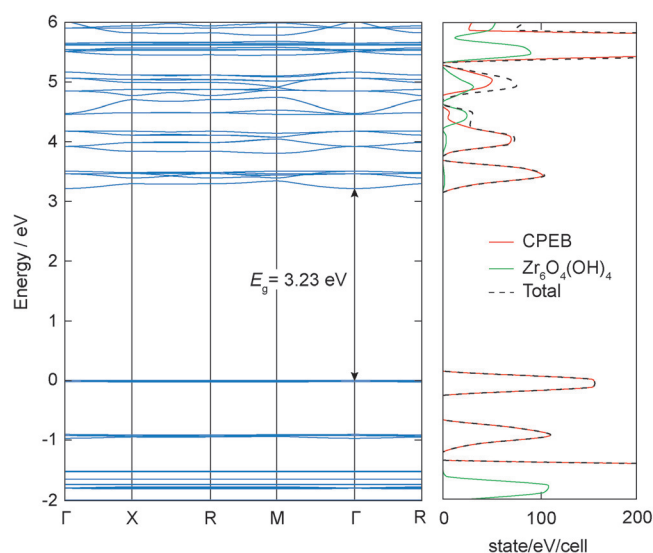


Figure 3. Calculated band structure in the first Brillouin zone and projected density of states of the non-interpenetrated VNU-1. The Fermi level is shifted at zero.

error is within the limitation of the DFT calculation in terms of band gap prediction. Additionally, the interpenetration observed in the real crystal structure can also play a contributing role to this difference. According to the DOS of VNU-1, both the valence band and conduction band are primarily composed of deprotonated CPEB linkers with little contribution arising from the Zr₆O₄(OH)₄(CO₂)₁₂ SBUs. This implicates the organic CPEB linker as playing an important role in effectively tuning the band gap of the resulting MOF material.^[16b,c,26] Our findings are consistent with the combined theoretical and experimental observations made for UiO-66 and MOF-5.^[26] It is noted that the conduction band of VNU-1 is very narrow whereas the valence band is wider. These findings are indicative of the fact that VNU-1 is a n-type semiconductor, similar to UiO-66 and UiO-66-NH₂.^[16b,26] Nevertheless, the significant extension of the absorption band of VNU-1-P into the visible-light region, in conjunction with the material's high chemical and water-stability, led us to investigate the UV/Vis driven photocatalytic performance of VNU-1-P for wastewater treatment.

Photocatalytic degradation of organic dye pollutants

In order to investigate the photocatalytic ability of VNU-1-P and VNU-2-P, two commonly used dyes, methylene blue (MB) and methyl orange (MO), were chosen as model dye pollutants in aqueous media. The photocatalytic performance of VNU-1-P and VNU-2-P in the UV/Vis light region was highlighted by the color variation (dark to light color) in the reaction system after as little as 30 min. The performances of the two photocatalysts were quantified by monitoring the disappearance in the absorbance bands of MB and MO at $\lambda_{\max} = 661$ and 464 nm, respectively, which is related to structural changes of the chromophoric unit of the dye molecules (Figure 4, Figure S14). The degradation rate profiles for the VNU-1-P photocatalytic system are shown in Figure 5, in which VNU-1-P is clearly ob-

| Table 2. Summary of the photoabsorption properties and pertinent structural information of VNU-1, VNU-2, and other related MOF structures. | | | | | |
|--|---|-----------------------|----------------|---------------------|-----------|
| MOF | SBU | Linker | Band Edge [nm] | Band Gap [eV] | Ref. |
| UiO-66 | Zr ₆ O ₄ (OH) ₄ (CO ₂) ₁₂ | BDC ^[a] | 305 | 4.07 | [19] |
| UiO-67 | Zr ₆ O ₄ (OH) ₄ (CO ₂) ₁₂ | BPDC ^[b] | 337 | 3.68 | [19] |
| MIL-125(Ti) | Ti ₈ O ₈ (OH) ₄ (CO ₂) ₆ | BDC | 345 | 3.60 | [13b] |
| UiO-66-Br | Zr ₆ O ₄ (OH) ₄ (CO ₂) ₁₂ | BDC(Br) | 360 | 3.44 | [13c] |
| VNU-2-P | Hf ₆ O ₄ (OH) ₄ (CO ₂) ₁₂ | CPEB | 369 | 3.36 | This work |
| UiO-68 | Zr ₆ O ₄ (OH) ₄ (CO ₂) ₁₂ | TPDC ^[c] | n.d. | 3.23 ^[d] | [18] |
| UiO-66-NO ₂ | Zr ₆ O ₄ (OH) ₄ (CO ₂) ₁₂ | BDC(NO ₂) | 400 | 3.10 | [13c] |
| VNU-1-P | Zr ₆ O ₄ (OH) ₄ (CO ₂) ₁₂ | CPEB | 430 | 2.88 | This work |
| UiO-66-NH ₂ | Zr ₆ O ₄ (OH) ₄ (CO ₂) ₁₂ | BDC(NH ₂) | 450 | 2.75 | [16b] |
| UiO-66(AN) | Zr ₆ O ₄ (OH) ₄ (CO ₂) ₁₂ | ANDC ^[e] | 502 | 2.47 | [20] |

[a] BDC = 1,4-benzenedicarboxylate; [b] BPDC = biphenyl-4,4'-dicarboxylate; [c] TPDC = [1,1':4',1''-terphenyl]-4,4''-dicarboxylate; [d] Based on density functional theory calculation; [e] ANDC = anthracene-9,10-dicarboxylate; n.d. = no experimental data available.

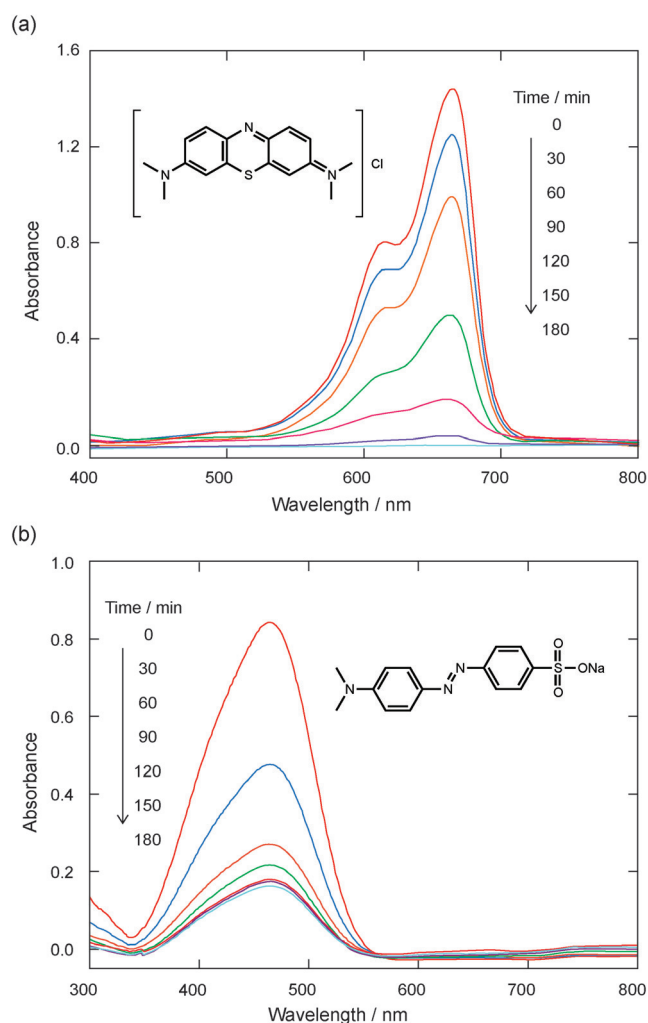


Figure 4. UV/Vis absorption spectra of the (a) MB and (b) MO solutions over the course of irradiation with UV/Vis light in the presence of VNU-1-P.

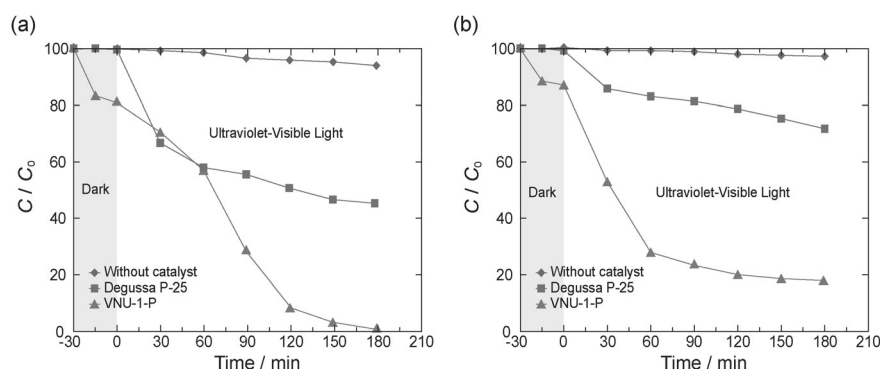


Figure 5. Degradation profiles of methylene blue (a) and methyl orange (b) under UV/Vis light by VNU-1-P (triangles), Degussa P-25 TiO₂ (squares), and no catalyst (diamonds, control experiment). The lines connecting the shapes are guides for the eyes.

served to have a higher activity than the commercially available Degussa P-25 TiO₂ under identical conditions. After 3 h, MB and MO were 100% and 83% degraded, respectively, by

the photocatalytic VNU-1-P. It is noted that these conversions are significantly higher than those observed for the comparison catalyst, Degussa P-25 TiO₂. These results are expected, as the absorbance band-edge of VNU-1-P is 430 nm and extends to about 540 nm, which allows VNU-1-P to absorb more visible light than the Degussa P-25 TiO₂. Moreover, we presume an additional reason for the higher activity of VNU-1-P is due to a larger accessible surface area, providing more photocatalytic active sites and promoting the transport of charge carriers.^[13c] In order to compare the performance of VNU-1-P with isorecticular structures that lack responsivity to UV/Vis light, control reactions were performed using UiO-66 and UiO-67 as the photocatalysts. From these reactions, it was clearly evident that UiO-66 and -67 displayed significantly less photocatalytic activity for dye degradation, thus highlighting the advantage of the visible-light-responsive VNU-1-P (Figure S15). Furthermore, an additional control experiment, without any catalyst present, demonstrated that both MB and MO were not able to be effectively photodegraded by UV/Vis light alone. In contrast to the highly active VNU-1-P photocatalyst, the photocatalytic activity of VNU-2-P was observed to be less effective than that of Degussa P-25 TiO₂ (Figure S16). The final concentration of MB and MO by VNU-2-P after irradiation for 3 h was calculated to be 53 and 72% of the initial concentration, respectively, which was expected due to the larger measured band gap for this material.

We reason that the photocatalytic degradation of MB and MO by VNU-1-P and VNU-2-P occurs via generation of electron-hole pairs under UV/Vis irradiation. Photoluminescence (PL) spectroscopy measurements, under 365 nm laser irradiation, display broad PL peaks for H₂CPEB, VNU-1-P, and VNU-2-P, which were centered at 432, 450, and 410 nm, respectively (Figure S17). The redshift and lower intensities observed for VNU-1-P in comparison to H₂CPEB indicate that electron-hole pairs were efficiently generated and separated.^[16b,c] Through

this mechanism, which is common amongst many photocatalytic MOF systems, hydroxyl radicals are produced as a result of a photoinduced energy transfer to adsorbed oxygen and water molecules.^[11,27] The resulting hydroxyl radicals effectively react and decompose MB and MO accordingly.^[11,27]

After photodegradation of the MB and MO dyes was completed (3 h), VNU-1-P and VNU-2-P were collected by centrifugation and washed three times with 20 mL of ethanol for a day. Following this, VNU-1-P and VNU-2-P were immersed in 20 mL of chloroform for a day, then filtered, and

subsequently regenerated under reduced pressure. PXRD analysis of the regenerated photocatalysts indicated that the crystallinity of these materials were retained (Figure 6, Figure S18).

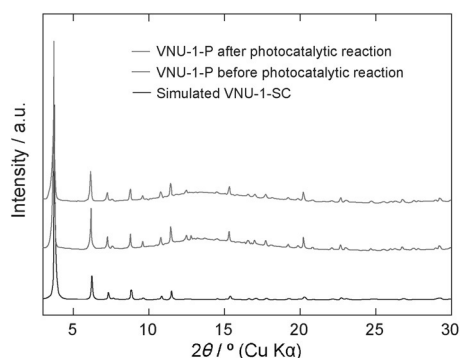


Figure 6. PXRD analysis of VNU-1-P before and after the photocatalytic degradation reaction in comparison to the calculated pattern from single-crystal data.

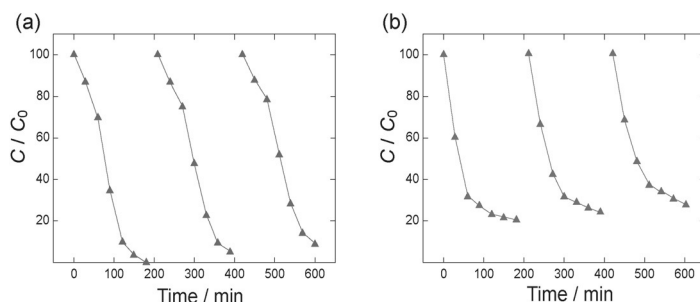


Figure 7. Degradation profiles of methylene blue (a) and methyl orange (b) by VNU-1-P over three consecutive cycles. The lines connecting the shapes are guides for the eyes.

This finding points to the remarkable stability of VNU-1-P and VNU-2-P under the aqueous reaction conditions. In order to demonstrate the recyclability of these heterogeneous photocatalysts, VNU-1-P and VNU-2-P were dispersed again in 100 ppm solutions of MB and MO. As shown in Figures 7 and S19, VNU-1-P and VNU-2-P exhibited efficient photodegradation of both MO and MB after three consecutive cycles. Specifically, the final relative concentrations of MO and MB were found to have decreased by only 10% over the course of three cycles.

Conclusions

Two novel heterogeneous MOF photocatalysts based on Zr^{IV} and Hf^{IV} inorganic SBUs and a highly π -conjugated linker were synthesized and their structures fully characterized. The structures of these MOFs, termed VNU-1 and VNU-2, respectively, were determined by single-crystal X-ray diffraction analyses, in which a doubly interpenetrated **fcu-c** net was found. By incorporating the highly π -conjugated linker, the optical absorption properties of VNU-1 were tuned to the visible-light region. In turn, this allowed VNU-1 to function as an effective heterogeneous photocatalyst in the UV/Vis light degradation of two model dye pollutant molecules, especially in comparison to the commercially available Degussa P-25 TiO_2 photocatalyst. Finally, VNU-1 was shown to remain crystalline after photocatalytic reactions were completed, and it was demonstrated that

VNU-1 was capable of being recycled, without appreciable loss of activity, for further use.

Experimental Section

Materials and general methods

Methyl 4-iodobenzoate, 1,4-diethynylbenzene, bis(triphenylphosphine)palladium dichloride, copper(I) iodide, potassium hydroxide, ammonium chloride (NH_4Cl), sodium chloride ($NaCl$), methylene blue (MB), methyl orange (MO), triethylamine (TEA), toluene, methanol (MeOH), acetic acid, chloroform, and *N,N*-dimethylformamide (DMF) were purchased from Aldrich Chemical Company. Zirconyl chloride octahydrate ($ZrOCl_2 \cdot 8H_2O$), hafnium chloride ($HfCl_4$), potassium hydroxide, and tetrahydrofuran (THF) were obtained from Acros Organics. P-25 TiO_2 was purchased from Degussa. All chemicals were used without further purification. Water used was double distilled and filtered through a millipore membrane. All experiments were performed in air.

1H and ^{13}C NMR spectra were acquired on a Bruker AVB-500 MHz spectrometer. High-resolution electrospray ionization mass spectra were obtained on a Bruker micrO-TOF-Q. Elemental microanalyses (EA) were performed in the Microanalytical Laboratory of the College of Chemistry at UC Berkeley, using a PerkinElmer 2400 Series II CHNS elemental analyzer. FT-IR spectra were analyzed from KBr pellets by using a Bruker Vertex 70 instrument. Thermal gravimetric analyses (TGA) were carried out on a TA Q500 Thermal Analysis System under airflow. Nitrogen adsorption isotherms at 77 K were measured on a Quantachrome Autosorb-iQ2, using helium of 99.999% purity for the estimation of dead space. Ultra-high-purity grade N_2 (99.999% purity) was used in the adsorption experiments. Optical microscopy images were acquired using a Nikon SMZ1000 microscope. UV-Vis diffuse reflectance spectra were recorded by using a JASCO V-670 UV-Vis spectrophotometer equipped with a diffuse reflectance accessory and barium sulfate as reference standard. UV-Vis spectra of photocatalytic dye degradation samples were collected on a JASCO V-670 spectrophotometer. Photoluminescence spectra were acquired on a Horiba Jobin Yvon spectrometer iHR320. Photocatalysis experiments were performed on an Oriol Newport system equipped with 300 W Xenon lamp.

Synthesis of 1,4-bis(2-[4-carboxyphenyl]ethynyl)benzene (H_2CPEB) linker

Synthesis of 1,4-bis(4-carbomethoxyphenylethynyl)benzene, precursor 1: Methyl 4-iodobenzoate (0.524 g, 2.00 mmol) and 1,4-diethynylbenzene (0.126 g, 1.00 mmol) were dissolved in a 50 mL Schlenk flask containing a 10 mL mixture of triethylamine and toluene ($v/v = 1:1$). Once dissolved, bis(triphenylphosphine)palladium dichloride (35.2 mg, 0.0500 mmol) and copper(I) iodide (2.0 mg, 10 μ mol) were then added in the reaction mixture. The solution was subsequently stirred at room temperature for 24 h. Next, the solvent was evaporated under reduced pressure and the remaining solid was washed consecutively with copious amounts of hexanes, a saturated solution of NH_4Cl , and a saturated solution of $NaCl$. The final pink product was dried under vacuum (0.335 g, 0.850 mmol, 85% yield). 1H NMR (500 MHz, $CDCl_3$, 25 °C, TMS): $\delta = 3.94$ (s, 6H), 7.54 (s, 4H), 7.59 (d, 4H, $J = 8.5$ Hz), 8.02 ppm (d, 4H, $J = 8.5$ Hz). ^{13}C NMR (125 MHz, $[D_6]DMSO$, 25 °C, TMS): $\delta = 165.92$, 131.74, 131.55, 129.76, 129.57, 127.33, 122.97, 91.38, 52.26 ppm.

MS (ESI) calculated for $C_{26}H_{18}O_4$: $m/z = 394.12$ ($[M+H]^+$); Found $m/z = 395.12$. FT-IR (KBr, 4000–400 cm^{-1}): $\tilde{\nu} = 2958$ (w), 2849 (br), 1721 (s), 1652 (w), 1636 (w), 1604 (m), 1558 (w), 1541 (w), 1518 (w), 1488 (w), 1435 (m), 1406 (m), 1375 (m), 1309 (m), 1281 (s), 1191 (m), 1176 (m), 1149 (m), 1107 (s), 955 (w), 857 (w), 838 (m), 810 (w), 768 (m), 697 (m), 549 (br), 524 (w), 490 (w), 419 cm^{-1} (w).

Synthesis of 1,4-bis(2-[4-carboxyphenyl]ethynyl)benzene (H_2CPEB) linker: Potassium hydroxide (0.420 g, 7.50 mmol) and 1,4-bis(4-carbomethoxyphenylethynyl)benzene (0.985 g, 0.250 mmol) were stirred in a mixture of methanol (3 mL), THF (3 mL) and water (1.5 mL) at room temperature overnight. After the reaction, the organic solvents were removed under reduced pressure, and the reaction solution was acidified by concentrated HCl to afford a faintly yellow precipitate. The final product was filtered once again, washed with copious amounts of water, and dried at 80 °C to yield 1,4-bis(2-[4-carboxyphenyl]ethynyl)benzene (0.0780 g, 0.213 mmol, 85% yield). 1H NMR (500 MHz, $[D_6]DMSO$, 25 °C, TMS): $\delta = 7.66$ (s, 4H), 7.68 (d, 4H, $J = 8.5$ Hz), 7.98 ppm (d, 4H, $J = 8.5$ Hz). ^{13}C NMR (125 MHz, $[D_6]DMSO$, 25 °C, TMS): $\delta = 166.61$, 131.88, 131.59, 130.79, 129.55, 126.22, 122.37, 91.34, 90.73 ppm. MS (ESI) calculated for $C_{24}H_{14}O_4$: $m/z = 366.09$ ($[M-H]^-$); found $m/z = 365.09$ FT-IR (KBr, 4000–400 cm^{-1}): $\tilde{\nu} = 3413$ (br), 3076 (br), 3039 (w), 3013(w), 2966 (w), 2842 (m, br), 2284 (w), 2214.34 (w), 1945 (w), 1927 (w), 1720 (s), 1602 (m), 1555 (m), 1516 (w), 1488 (w), 1433 (m), 1405 (m), 1375 (m), 1310 (m), 1281 (s), 1190 (m), 1174 (m), 1148 (m), 1105 (s), 1015 (m), 952 (m), 859 (m), 837 (m), 809 (m), 768 (m), 696 (m), 547 (m), 522 (w), 489 (m), 450 (w), 423 cm^{-1} (w).

Synthesis of $[Zr_6O_4(OH)_4(CPEB)_6]$ (VNU-1) and $[Hf_6O_4(OH)_4(CPEB)_6]$ (VNU-2)

Synthesis of single crystals of $[Zr_6O_4(OH)_4(CPEB)_6]$, VNU-1-SC (where SC = single crystal): $ZrOCl_2 \cdot 8H_2O$ (10.9 mg, 0.0340 mmol) and H_2CPEB (12.4 mg, 0.0340 mmol) were dissolved in DMF (3.80 mL) in a 10 mL capped vial with acetic acid (0.2 mL) added as a modulator. The solution was subsequently heated at 120 °C for 3 days in an isothermal oven to yield a colorless crystalline solid. After cooling the vial to room temperature, the crystalline product was separated from the mother liquor via centrifugation (40% yield based on the H_2CPEB linker). The single crystals collected were then used for single-crystal X-ray diffraction analysis.

Synthesis of microcrystalline $[Zr_6O_4(OH)_4(CPEB)_6]$ powder, VNU-1-P (where P = powder): $ZrOCl_2 \cdot 8H_2O$ (10.9 mg, 0.0340 mmol) and H_2CPEB (12.4 mg, 0.0340 mmol) were dissolved in a solvent mixture of DMF (3.86 mL), acetic acid (0.042 mL), and water (0.10 mL) in a 10 mL capped vial. The solution was subsequently heated at 120 °C for 1 day in an isothermal oven to yield a yellow precipitate. After cooling the vial to room temperature, the yellow precipitate product, VNU-1-P, was separated from the mother liquor via centrifugation (68% yield based on the H_2CPEB linker). The as-synthesized sample of VNU-1-P was washed with 10 mL of DMF three times per day over the course of three days. Following this, VNU-1-P was immersed in 10 mL chloroform, which was replaced three times per day for a total of three days. After the solvent-exchange process was completed, VNU-1-P was activated under reduced pressure at 120 °C for 24 h. Elemental anal. calcd for $Zr_6C_{144}H_{76}O_{32} = [Zr_6O_4(OH)_4(C_{24}H_{12}O_4)_6]$: C, 60.35; H, 2.67%; found: C, 56.94; H, 2.63; N, 0.23%. Calcd. for $Zr_6C_{143.3}H_{95.6}N_{0.5}O_{40.8} = [Zr_6O_4(OH)_4(C_{24}H_{12}O_4)_{5.9}(C_2H_3O_2)_{0.1}] \cdot 3(H_2O) \cdot 0.5 DMF$: C, 58.86; H, 2.92; N, 0.24%. FT-IR (KBr, 4000–400 cm^{-1}): $\tilde{\nu} = 1657$ (m), 1602 (m), 1544 (m), 1413 (s), 1179 (w), 1102 (w), 1016 (w), 860 (w), 835 (w), 780 (m), 697 (w), 663 (w), 478 cm^{-1} (w).

Synthesis of single crystals of $[Hf_6O_4(OH)_4(CPEB)_6]$, VNU-2-SC: $HfCl_4$ (10.9 mg, 0.0340 mmol) and H_2CPEB (12.4 mg, 0.0340 mmol) were dissolved in DMF (3.75 mL) in a 10 mL capped vial with acetic acid (0.25 mL) added as a modulator. The solution was subsequently heated at 120 °C for 3 days in an isothermal oven to yield a colorless crystalline solid. After cooling the vial to room temperature, the crystalline product was separated from the mother liquor via centrifugation (35% yield based on the H_2CPEB linker). The single crystals collected were then used for single-crystal X-ray diffraction analysis.

Synthesis of microcrystalline $[Hf_6O_4(OH)_4(CPEB)_6]$ powder, VNU-2-P: $HfCl_4$ (10.9 mg, 0.0340 mmol) and H_2CPEB (12.4 mg, 0.0340 mmol) were dissolved in a solvent mixture of DMF (3.80 mL), acetic acid (0.10 mL), and water (0.10 mL) in a 10 mL capped vial. The solution was subsequently heated at 120 °C for 3 days in an isothermal oven to yield light yellow microcrystalline powder. After cooling the vial to room temperature, the light yellow solid product, VNU-2-P, was separated from the mother liquor via centrifugation (59% yield based on the H_2CPEB linker). The as-synthesized sample of VNU-2-P was washed with 10 mL of DMF three times per day over the course of three days. Following this, VNU-2-P was immersed in 10 mL chloroform, which was replaced three times per day for a total of three days. After the solvent-exchange process was completed, VNU-2-P was activated under reduced pressure at 120 °C for 24 h. Elemental anal. calcd for $Hf_6C_{144}H_{76}O_{32} = [Hf_6O_4(OH)_4(C_{24}H_{12}O_4)_6]$: C, 51.09; H, 2.27%; found: C, 52.08; H, 2.67; N, 0.30%. Calcd. for $Hf_6C_{145.5}H_{79.5}N_{0.5}O_{32.5} = [Hf_6O_4(OH)_4(C_{24}H_{12}O_4)_6] \cdot 0.5 DMF$: C, 51.01; H, 2.34; N, 0.29%. FT-IR (KBr, 4000–400 cm^{-1}): $\tilde{\nu} = 1656$ (m), 1604 (m), 1544 (m), 1496 (m), 1409 (s), 1391 (s), 1253 (w), 1163 (w), 1099 (w), 1065 (w), 920 (w), 773 (w), 720 (w), 667 (m), 548 cm^{-1} (w).

X-ray diffraction analysis

A single crystal of VNU-1-SC or VNU-2-SC was isolated from the mother liquor of the reaction by a nylon loop and mounted. The X-ray diffraction data for these materials were both collected on a Bruker D8 Venture diffractometer outfitted with a PHOTON-100 CMOS detector using monochromatic microfocus $Cu_{K\alpha}$ radiation ($\lambda = 1.54178$ Å) that was operated at 50 kW and 1.0 mA. The VNU-1-SC data was collected at room temperature whereas VNU-2-SC was cooled down to 100 K by chilled nitrogen flow controlled by a Kryoflex II system before data collection. Unit cell determination was performed in the Bruker SMART APEX II software suite. The data sets were reduced and a multi-scan spherical absorption correction was implemented in the SCALE interface.^[28] The structures were solved with direct methods and refined by the full-matrix least-squares method in the SHELXL-97 program package.^[29] Once the framework atoms were located in the difference Fourier maps, the SQUEEZE routine in PLATON was performed to remove scattering from disordered guest molecules residing in the pores.^[24] Detailed descriptions of structural refinement can be found in Tables S1 and S2 in the Supporting Information. Crystallographic data for VNU-1-SC and VNU-2-SC have been deposited in the Cambridge Crystallographic Data Centre (deposition numbers: 1063477 and 1063478). This data can be obtained, free of charge, via the web (www.ccdc.cam.ac.uk/data_request/cif). PXRD patterns were collected using a Bruker D8 Advance equipped with a Ni filtered $Cu_{K\alpha}$ radiation ($\lambda = 1.54178$ Å) source. The diffractometer was also outfitted with an anti-scattering shield that prevented incident diffuse radiation from hitting the detector. Sample preparation included placing samples of VNU-1-P and VNU-2-P on a zero background holder and flattening them with a spatula. The 2θ range was 3–30° with a step size of 0.02° and a fixed counting time of 0.3 s/step.

Computational methods

Theoretical calculations have been carried out at the B3LYP level of theory with the Gaussian-type functions (GTFs) CRYSTAL program.^[30] All electron basis set was used for Zr and the triple-zeta valence basis sets with polarization quality were employed for H, C, O.^[31] The reciprocal space is represented using the Monkhorst-Pack scheme with a $2 \times 2 \times 2$ k -mesh. For the structural optimization, the convergence criteria for SCF energy and RMS on displacements were set to 10^{-10} a.u. and 0.00012 a.u., respectively. The symmetry of the structure was maintained during the relaxation. The non-interpenetrated version of VNU-1 (cubic, space group $F-43m$, No. 216) was used in the calculation. The calculated lattice constant 40.2147 Å agrees well with the experimental value of 39.8961 Å, suggesting that the interpenetration does not significantly change the unit cell parameters of this structure.

Evaluation of photocatalytic activity

In order to assess the photocatalytic properties of VNU-1-P and VNU-2-P for dye pollutant degradation, VNU-1-P or VNU-2-P (10 mg) was dispersed in a 20 mL quartz tube containing a 15 mL aqueous solution of the appropriate dye (100 ppm concentration). The water used for the experiment was doubly distilled and filtered through a Millipore membrane. Prior to initiating the photocatalytic reactions, the mixture was stirred for 30 min at 25 °C in the dark in order to establish equilibrium and effectively disperse the photocatalyst. The quartz tube was then placed at a fixed position of 18 cm from the light source and adequate stirring was maintained. The reaction mixture was then irradiated at 25 °C under a 300 W xenon lamp equipped with an IR cutting filter to cut off light with wavelengths > 750 nm and a light intensity of 400 mW cm^{-2} . Sample aliquots were collected at regular intervals and were treated by filtration through a Millipore membrane, followed by centrifugation to remove the small amount of remaining VNU-1-P catalyst particle contaminants. The concentration of MB or MO were monitored by measuring the absorbance intensity at their maximum absorbance wavelengths of $\lambda_{\text{max}} = 661$ and 464 nm, respectively, as determined by calibration based on the Beer-Lambert law prior to the photocatalyst measurements. Control (no photocatalyst) and comparison (Degussa P-25 TiO_2) experiments were performed following the same procedure.

Acknowledgements

We acknowledge the financial support provided by Vietnam National University, Ho Chi Minh City (Nos. B2014-50-01, A2015-50-01-HĐ-KHCN, and MANAR-CS2014-02), and ONRG-NICOP (No. N62909-15-1N056). We gratefully acknowledge the use of computational resources of the HPCI system provided by Cyberscience Center, Tohoku University through the HPCI System Research (project ID:hp150084). We thank Ms. A. M. Osborn, Dr. H. Furukawa, Prof. H. T. Nguyen, Mr. T. N. Tu, and Ms. L. H. T. Nguyen at MANAR for their valuable discussions. Furthermore, we appreciate Mr. C. Tischler and Prof. J. K. Kang at Korea Advanced Institute of Science and Technology (KAIST) for advice and instrument use during the early stages of this work. Finally, we acknowledge Prof. O. M. Yaghi (UC Berkeley) for starting and supporting the Center for Molecular and Nano-Architecture.

Keywords: dye degradation · heterogeneous catalysis · photocatalysis · porous materials · wastewater treatment

- [1] a) K. Sarayu, S. Sandhya, *Appl. Biochem. Biotechnol.* **2012**, *167*, 645–661; b) S. Şen, G. N. Demirel, *Water Res.* **2003**, *37*, 1868–1878; c) J. J. Plumb, J. Bell, D. C. Stuckey, *Appl. Environ. Microbiol.* **2001**, *67*, 3226–3235.
- [2] a) I. Nilsson, A. Möller, B. Mattiasson, M. S. T. Rubindamayugi, U. Welandner, *Enzyme Microb. Technol.* **2006**, *38*, 94–100; b) J. Swamy, J. A. Ramsay, *Enzyme Microb. Technol.* **1999**, *24*, 130–137.
- [3] a) M. A. Rauf, S. Salman Ashraf, *Chem. Eng. J.* **2009**, *151*, 10–18; b) D. S. Bhatkhande, V. G. Pangarkar, A. A. Beenackers, *J. Chem. Technol. Biotechnol.* **2002**, *77*, 102–116.
- [4] a) S. Sakthivel, B. Neppolian, M. V. Shankar, B. Arabindoo, M. Palanichamy, V. Murugesan, *Sol. Energy Mater. Sol. Cells* **2003**, *77*, 65–82; b) W. L. Kostedt, A. A. Ismail, D. W. Mazyck, *Ind. Eng. Chem. Res.* **2008**, *47*, 1483–1487.
- [5] a) W. Zhao, W. Ma, C. Chen, J. Zhao, Z. Shuai, *J. Am. Chem. Soc.* **2004**, *126*, 4782–4783; b) H. S. Jung, Y. J. Hong, Y. Li, J. Cho, Y. J. Kim, G. C. Yi, *ACS Nano* **2008**, *2*, 637–642.
- [6] H. Furukawa, K. E. Cordova, M. O’Keeffe, O. M. Yaghi, *Science* **2013**, *341*, 1230444.
- [7] a) Y. He, W. Zhou, G. Qian, B. Chen, *Chem. Soc. Rev.* **2014**, *43*, 5657–5678; b) J. A. Mason, M. Veenstra, J. R. Long, *Chem. Sci.* **2014**, *5*, 32–51; c) Y.-B. Zhang, H. Furukawa, N. Ko, W. Nie, H. J. Park, S. Okajima, K. E. Cordova, H. Deng, J. Kim, O. M. Yaghi, *J. Am. Chem. Soc.* **2015**, *137*, 2641–2650; d) J.-R. Li, J. Sculley, H.-C. Zhou, *Chem. Rev.* **2012**, *112*, 869–932.
- [8] a) J. Liu, P. K. Thallapally, B. P. McGrail, D. R. Brown, J. Liu, *Chem. Soc. Rev.* **2012**, *41*, 2308–2322; b) N. T. T. Nguyen, H. Furukawa, F. Gándara, H. T. Nguyen, K. E. Cordova, O. M. Yaghi, *Angew. Chem. Int. Ed.* **2014**, *53*, 10645–10648; *Angew. Chem.* **2014**, *126*, 10821–10824.
- [9] J. Liu, L. Chen, H. Cui, J. Zhang, L. Zhang, C.-Y. Su, *Chem. Soc. Rev.* **2014**, *43*, 6011–6061.
- [10] Z. Hu, B. J. Deibert, J. Li, *Chem. Soc. Rev.* **2014**, *43*, 5815–5840.
- [11] a) T. Zhang, W. Lin, *Chem. Soc. Rev.* **2014**, *43*, 5982–5993; b) C.-C. Wang, J.-R. Li, X.-L. Lv, Y.-Q. Zhang, G. Guo, *Energy Environ. Sci.* **2014**, *7*, 2831–2867; c) R. Li, X. Ren, H. Ma, X. Feng, Z. Lin, X. Li, C. Hu, B. Wang, *J. Mater. Chem. A* **2014**, *2*, 5724–5729; d) Y. Zhang, X. Feng, H. Li, Y. Chen, J. Zhao, S. Wang, L. Wang, B. Wang, *Angew. Chem. Int. Ed.* **2015**, *54*, 4259–4263; *Angew. Chem.* **2015**, *127*, 4333–4337.
- [12] a) H. Q. Pham, T. Mai, N.-N. Pham-Tran, Y. Kawazoe, H. Mizuseki, D. Nguyen-Manh, *J. Phys. Chem. C* **2014**, *118*, 4567–4577; b) M. Fuentes-Cabrera, D. M. Nicholson, B. G. Sumpter, M. Widom, *J. Chem. Phys.* **2005**, *123*, 124713; c) L. Shen, S. Liang, W. Wu, R. Liang, L. Wu, *Dalton Trans.* **2013**, *42*, 13649–13657.
- [13] a) M. Alvaro, E. Carbonell, B. Ferrer, F. X. Labrés i Xamena, H. Garcia, *Chem. Eur. J.* **2007**, *13*, 5106–5112; b) C. H. Hendon, D. Tiana, M. Fontecave, C. Sanchez, L. D’arras, C. Sassoie, L. Rozes, C. Mellot-Draznieks, A. Walsh, *J. Am. Chem. Soc.* **2013**, *135*, 10942–10945; c) L. Shen, R. Liang, M. Luo, F. Jing, L. Wu, *Phys. Chem. Chem. Phys.* **2015**, *17*, 117–121.
- [14] M. Dan-Hardi, C. Serre, T. Frot, L. Rozes, G. Maurin, C. Sanchez, G. Férey, *J. Am. Chem. Soc.* **2009**, *131*, 10857–10859.
- [15] J. H. Cavka, S. Jakobsen, U. Olsbye, N. Guillou, C. Lamberti, S. Bordiga, K. P. Lillerud, *J. Am. Chem. Soc.* **2008**, *130*, 13850–13851.
- [16] a) C. Gomes Silva, I. Luz, F. X. Labrés i Xamena, A. Corma, H. Garcia, *Chem. Eur. J.* **2010**, *16*, 11133–11138; b) J. Long, S. Wang, Z. Ding, S. Wang, Y. Zhou, L. Huang, X. Wang, *Chem. Commun.* **2012**, *48*, 11656–11658; c) D. Sun, Y. Fu, W. Liu, L. Ye, D. Wang, L. Yang, X. Fu, Z. Li, *Chem. Eur. J.* **2013**, *19*, 14279–14285; d) T. W. Goh, C. Xiao, R. V. Maligal-Ganesh, X. Li, W. Huang, *Chem. Eng. Sci.* **2015**, *124*, 45–51.
- [17] a) Y. Fu, D. Sun, Y. Chen, Z. Ding, X. Fu, Z. Li, *Angew. Chem. Int. Ed.* **2012**, *51*, 3364–3367; *Angew. Chem.* **2012**, *124*, 3420–3423; b) Y. Horiuchi, T. Toyao, M. Saito, K. Mochizuki, M. Iwata, H. Higashimura, M. Anpo, M. Matsuoka, *J. Phys. Chem. C* **2012**, *116*, 20848–20853; c) M. A. Nasalevich, M. G. Goesten, T. J. Savenije, F. Kapteijn, J. Gascon, *Chem. Commun.* **2013**, *49*, 10575–10577; d) M. de Miguel, F. Ragon, T. Devic, C. Serre, P. Horcajada, H. Garcia, *ChemPhysChem* **2012**, *13*, 3651–3654; e) S.-N. Kim, H.-Y. Kim, H.-Y. Cho, W.-S. Ahn, *Catal. Today* **2013**, *204*, 85–93.

- [18] L.-M. Yang, E. Ganz, S. Svelle, M. Tilset, *J. Mater. Chem. C* **2014**, *2*, 7111–7125.
- [19] S. Chavan, J. G. Vitillo, D. Gianolio, O. Zavorotynska, B. Civalleri, S. Jacobsen, M. H. Nilsen, L. Valenzano, C. Lamberti, K. P. Lillerud, S. Bordiga, *Phys. Chem. Chem. Phys.* **2012**, *14*, 1614–1626.
- [20] S. Pu, L. Xu, L. Sun, H. Du, *Inorg. Chem. Commun.* **2015**, *52*, 50–52.
- [21] T. M. Fasina, J. C. Collings, J. M. Burke, A. S. Batsanov, R. M. Ward, D. Albesa-Jové, L. Porrès, A. Beeby, J. A. K. Howard, A. J. Scott, W. Clegg, S. W. Watt, C. Viney, T. B. Marder, *J. Mater. Chem.* **2005**, *15*, 690–697.
- [22] A. Schaate, P. Roy, A. Godt, J. Lippke, F. Waltz, M. Wiebcke, P. Behrens, *Chem. Eur. J.* **2011**, *17*, 6643–6651.
- [23] A. Schaate, P. Roy, T. Preuse, S. J. Lohmeier, A. Godt, P. Behrens, *Chem. Eur. J.* **2011**, *17*, 9320–9325.
- [24] A. L. J. Spek, *J. Appl. Crystallogr.* **2003**, *36*, 7–13.
- [25] It is noted that the absence of strong absorption at 200 nm accompanied by the long absorption tail from 500–700 nm in the UV-DRS spectra of VNU-1-P points to the possible presence of luminescent carbonaceous impurities. The decomposition of DMF to form guest oligomers that are not easily removed by vacuum may be the cause for this. S. S. Kaye, A. Dailly, O. M. Yaghi, J. R. Long, *J. Am. Chem. Soc.* **2007**, *129*, 14176–14177.
- [26] a) L. Valenzano, B. Civalleri, S. Chavan, S. Bordiga, M. H. Nilsen, S. Jacobsen, K. Lillerud, C. Lamberti, *Chem. Mater.* **2011**, *23*, 1700–1708; b) B. Civalleri, F. Napoli, Y. Noël, C. Roetti, R. Dovesi, *CrystEngComm* **2006**, *8*, 364–371; c) S. Bordiga, C. Lamberti, G. Ricchiardi, L. Regli, F. Bonino, K.-P. Lillerud, M. Bjorgen, A. Zecchina, *Chem. Commun.* **2004**, 2300–2301.
- [27] a) C. Galindo, P. Jacques, A. Kalt, *J. Photochem. Photobiol. A* **2000**, *130*, 35–47; b) J. Joseph, H. Destailhats, H. Hung, M. Hoffmann, *J. Phys. Chem. A* **2000**, *104*, 301–307; c) A. Houas, H. Lachheb, M. Ksibi, E. Elaloui, C. Guillard, J. Herrmann, *Appl. Catal. B* **2001**, *31*, 145–157; d) M. C. Das, H. Xu, Z. Wang, G. Srinivas, W. Zhou, Y. Yue, V. N. Nesterov, G. Qian, B. Chen, *Chem. Commun.* **2011**, *47*, 11715–11717.
- [28] C. H. Görbitz, *Acta Crystallogr. Sect. B* **1999**, *55*, 1090–1098.
- [29] G. M. Sheldrick, SHELXL97, Program for Crystal Structure Refinement, University of Göttingen, Göttingen (Germany), **1997**.
- [30] R. Dovesi, V. R. Saunders, R. Roetti, R. Orlando, C. M. Zicovich-Wilson, F. Pascale, B. Civalleri, K. Doll, N. M. Harrison, I. J. Bush, P. D'Arco, M. Llunell, CRYSTAL09, University of Torino, Torino (Italy), **2009**.
- [31] M. F. Peintinger, D. V. Oliveira, T. Bredow, *J. Comput. Chem.* **2013**, *34*, 451–459.

Manuscript received: June 21, 2015

Revised: July 31, 2015

Accepted Article published: August 10, 2015

Final Article published: September 4, 2015